Journal of Sound and Vibration (2001) **239**(4), 695–708
doi:10.1006/jsvi.2000.3223, available online at http://www.idealibrary.com on IDEAL®

THE OBSERVED AEROACOUSTIC BEHAVIOUR OF SOME FLOW-EXCITED EXPANSION CHAMBERS

P. O. A. L. Davies and K. R. Holland

Institute of Sound and Vibration Research, University of Southampton, Southampton SO17 1 BJ, England

(*Accepted* 24 *July* 2000)

Expansion chambers are often installed in flow duct systems to reduce pressure pulsations and to act as silencers. However, in certain circumstances they can become flow-excited sound generators rather than attenuators. The physics of the flow acoustic interactions responsible for this are examined in detail. They are then illustrated by a systematic sequence of sound power flux measurements in the downpipe, expansion chamber and tailpipe of some representative examples. These measurements then identify both the position and spectral characteristics of the sources of sustained excitation by the flow in its relation to the local geometry and its associated reverberant acoustic behaviour.

1. INTRODUCTION

Almost immediately after he took up the Hawker Siddeley Lectureship in Accoustics on April Fool's day in 1962, Philip Doak joined the first author in drafting the documents supporting proposals to the University for the establishment of a Noise and Vibration Research Institute and later, those encouraging its incorporation as a new department of the Faculty of Engineering. As well as developing a mission statement for the Institute of Sound and Vibration Research (ISVR), we were charged with producing the submissions to the then Department of Scientific and Industrial Research (DSIR) for a major grant to develop the Institute and its work in applied acoustics and noise control. This established a pattern of working together from time to time on topics of common interest that has continued to flourish ever since, reinforced perhaps by our common war service background in radar and our lifetime practical interest in making music. One such topic is concerned with experimental, theoretical and numerical studies of the appropriate combinations of fluid dynamics and acoustics [1–4] that describe the propagation of acoustic energy through flow ducts and pipes and also with those local physical processes responsible for the generation of sound by unsteady separating flow.

The sustained excitation of a tuned resonator by shed vorticity in a separating shear layer [5], or the whistling produced by the impingement of thin fluid jets on an edge [6] have both been exploited by the makers of musical instruments from time immemorial. Familiar examples include pan pipes, recorders, flutes, organ flue pipes [5–7], aeolian tones and so on. Over the centuries, the acquisition of the necessary knowledge and skill for their successful production must have been laboriously accomplished by much trial and error. A more physically explicit understanding [5–7] of the basic controlling mechanisms began to emerge during the great upsurge in scientific observation and discovery from the mid-19th century, as this was also accompanied by the relevant developments in acoustics

0022-460X/01/040695 + 14 $35.00/0

and fluid mechanics. These mechanisms can take several forms [8–15], depending on subtle differences in local and overall geometric detail and its relation to the magnitude, direction and distribution of the impinging flow. One such form includes many examples of reverberant flow duct systems, where separating shear layers [4] can form at junctions, expansions, orifices and the like, providing the conditions where this coupled flow acoustic behaviour may occur [4, 10–16]. It is well known [5] that whenever a flow leaves a downstream facing edge it separates, forming a thin shear layer or vortex sheet. Such sheets, which involve high transverse velocity gradients, are very unstable and rapidly develop waves which roll up to form an ordered train of vortices [4–14, 16, 17]. Flow separations may also occur at upstream facing corners, but the flow may re-attach before an ordered set of vortices can form.

The prediction and control of flow-generated noise represents a current controlling factor [12] in the design of automotive exhaust systems that reduce engine breathing noise emissions to levels that comply with legislation or meet customer expectations. Realistic descriptions of sound emissions from confined sources in flow ducts [4, 10, 12, 16] require that due account is included for the reverberant influence of the boundaries on the transfer of acoustic energy from the sources and its subsequent transmission to the point of emission and radiation to the environment. Although sound propagation in flow ducts is sufficiently well understood and documented [12, 16], the lack of essential detail [4, 16] ensures that sufficiently comprehensive predictive models for quantifying all types of flow noise sources found in pipe networks do not currently exist, though they may do so for some specific cases [4, 12–15]. Some recent observations providing further details of the aeroacoustic behaviour of flow-excited expansion chambers are described in what follows here. These form one part of an experimental programme that was undertaken to provide quantitative descriptions that can be incorporated into existing noise emission predictive software [16, 18] that runs on a personal computer (PC) and is thus widely accessible.

1.1. EXPANSION CHAMBER SILENCERS

Expansion chambers are often installed in the intake and exhaust ducts of IC engines and reciprocating compressors to reduce the amplitude of the cyclic flow pulsations generated as an essential feature of their operation. The intention is to reduce the associated sound emissions from their open orifices and vibrating surfaces by smoothing the pulsations and reducing the propagation of wave energy through them. For similar reasons, such acoustic silencing elements are often included in pipe and duct networks transporting pulsating fluids during industrial operations. Their acoustic behaviour is normally strongly reactive, the primary controlling factors being their length and expansion ratio with the acoustic impedance at their outlet contraction. This behaviour is often strongly modified [16] by the addition of internal components such as annular sidebranches, perforated pipes and baffles, orifices, and external ones such as attached resonators [4] and tailpipes, etc. Observations have also shown that, in appropriate circumstances, such an expansion chamber in a flow duct may also behave as a source of sound at frequencies related to the acoustic resonances of its tailpipe [10–12], or of its intake pipe [8]. Apparently, this normally arises from the impingement at their downstream or outlet contraction edge [8–12] of the train of coherent vortices produced by the rolling up of the vortex sheets shed from the lip of their inlet at the upstream end of the expansion. This process often occurs periodically at a rate controlled by the acoustic resonances of the system. See, for example, Figure 6 of both references [10, 12]. This behaviour was also clearly demonstrated [13, 14] during detailed studies of the self-excitation of a resonator by flow across its neck opening.

It appears somewhat paradoxical that expansion chambers installed in flow ducts possess the potential to become generators rather than sound attenuators, thus frustrating the purpose for which they were installed. The somewhat diffuse sustained hum emitted by some flow-excited expansion chamber/tailpipe combinations situated at the open end of flow ducts is often clearly audible, so long as the background level remains sufficiently low. There is also clear evidence [10, 12, 16, 18] that acoustically controlled vortex shedding in an expansion chamber is responsible for it acting as an amplifier of sound incident on it from upstream. The conditions under which such behaviour becomes obvious apparently depends in a non-linear manner on several factors such as the flow Mach number, the incident sound intensity and the acoustic reflective properties of the chamber outlet boundary. This aspect of expansion chamber acoustics is not considered further here, except to note that the addition on an appropriately perforated pipe [4, 16], bridging between its inlet and outlet, can substantially improve attenuation performance, presumably by suppressing flow separation with the subsequent formation of a coherent train of vortices.

1.2. SOME EXAMPLES OF FLOW-EXCITED RESONANCE

As a consequence of their inherent complexity and generally non-linear dynamic behaviour, such separating and impinging vortical flows, together with the acoustic energy they generate, have often proved extremely difficult to model adequately from first principles. Thus, one has normally been obliged to accept some appropriate and often somewhat drastic simplifying assumptions during the analytic development.

Recently, Doak [1] has presented a rigorous general formulation that describes both the propagation and aerodynamic generation of sound by various disturbances in a flowing fluid. Although comprehensive, many of the controlling fundamental features of the flow included in this formulation are difficult to quantify sufficiently explicitly, either by calculation or measurement, to apply directly to many practical situations of interest. However, the application of a simplified one-dimensional version of this approach, combined with appropriate acoustic modelling, often restricted to plane axially propagating waves [4, 10, 12], has already provided predictions that are in close or fair agreement with observations. In such cases and some others [8, 11], sustained oscillations were maintained at frequencies f_r apparently controlled by eddy shedding at frequencies corresponding to the acoustic resonances of adjacent lengths of pipe. This can then be expressed simply by

$$f_r = 2nc_0/L_r, \quad n = 1, 2, 3, \ldots, \tag{1}$$

where c_0 is the local sound speed and L_r is the effective length of the resonator. However, in most cases their amplitude was determined by direct measurement, or alternatively, but not always [10, 12–15], required some empirically determined factors for its estimation.

There are many flow-excited examples of the generation of a sequence of tones where the frequency changes in discrete steps as the flow speed increases. This behaviour has often been known as staging. Observations [8] indicate that a controlling influence is due to the development of growing instability waves in separating shear layers, or by wave-like transverse displacement growing along thin planar jets. Examples where this represents the controlling mechanism include edge tones [6–9], many flow-excited Helmholtz resonators [8, 9], simple cut-outs and cavities [8] and finally, of expansion chambers without a tailpipe

[8, 11], where the frequency of sustained oscillation f_c, normally exhibits staging. This may then be expressed by

$$f_c = ((n \pm \varepsilon)/L)(1/(1 + M_c)), \quad n = 1, 2, 3 \ldots, \tag{2}$$

where $0 < \varepsilon < 0{\cdot}5$ represents the influence of phase delays associated with the formation or impingement of instability waves or their equivalent, the convective Mach number $M_c = U_c/c_0$, where U_c is the phase or convection velocity of the disturbances, while L is the effective path length over which both acoustic and hydrodynamic disturbances travel. This then represents a feedback interaction of flow instability and a single resonant acoustic mode, yielding a frequency that varies with flow velocity.

Such self-excited flow oscillations are common examples of non-linear systems [15] that possess limit cycles and can also be understood in terms of a feedback process [4–14]. It can be shown [15] that feedback descriptions of flow resonator systems are complementary to analytic descriptions that employ describing function analysis. This was applied [15] to the flow-induced acoustic oscillation of a resonator [13, 14], by a grazing boundary layer flow across its neck opening. Non-linearity was assumed [15] to be associated with the initial growth and later saturation of the flow disturbances that were responsible for exciting an otherwise linear system. The describing function for the non-linearly saturated flow disturbance was estimated [15] by making use of experimental observations with several flow resonant systems including those in references [8, 13]. The resulting describing function combined with a similar function giving the measured linear response of the resonator [13] determined the amplitude, frequency and mean flow characteristics for the limit cycle oscillations. Sufficiently detailed measurements and relevant descriptive data were available [13] to calculate from first principles, the variation of the values of flow-excited oscillation frequency and normalized oscillation velocity amplitude, as determined by the value of the free-stream velocity. The calculated frequency always agreed closely with the observed values [13, 15] as indeed did the general shape of the variation of velocity amplitude with the mean flow velocity. However, the calculated peak value occurred at a flow velocity across the neck that was some 8% above the experimental one of 12 m/s. This corresponded to a Strouhal number fL/U of 0·5 [10, 13], equivalent to a vortex spacing of $2L$, expressed simply by

$$fL/U = (m - 0{\cdot}5), \quad m = 1, 2, 3, \ldots, \tag{3}$$

when m is unity in this case. In this example, L also corresponded to the streamwise length of the resonator neck opening!

A rather different approach [14] set out to describe the physics of the flow acoustic interaction in terms of the detailed momentum and energy exchanges occurring inside the fluid. The total flow field was regarded as the superposition of a purely vortical flow field, directly associated with shed vorticity and a potential flow, of which the unsteady part was associated with acoustic resonance. Experimental results [13] provided some essential information on the principal features of these two flow fields, with the dynamics of their interaction. The picture that emerged [14] suggests that vorticity in the separating flow is concentrated into a train of discrete vortices by Coriolis acceleration [1] arising from the interactions between the shear layer with the local potential flow or acoustic velocity fluctuations. It was then argued [14] that the degree of concentration of vorticity in each member of the train increases with the amplitude of these acoustic velocity fluctuations, that reaches a maximum at acoustic resonance. The vortices then convect to the downstream edge, where a similar interaction mechanism [1, 14] extracts energy from the mean flow at a rate that increases rapidly with vorticity concentration. Some energy is carried away by

the vortices, some makes up for any acoustic losses, that will also include the power radiated to the far field, while a proportion is fed back upstream to assist in the formation of new vortices. As vorticity concentration increases, with any rise in source sound level, a limit is reached where the energy extracted from the mean flow remains in balance with the sum of all the losses, including any acoustic emissions, thus maintaining a constant acoustic excitation.

2. FLOW-EXCITED EXPANSION CHAMBERS

A similar sequence can describe the physics of the flow–acoustic interactions responsible for sound generation in flow-excited expansion chambers. Some details will obviously differ since the velocity field is now axisymmetric not plane as in reference [14]. Consequently, a cylindrical co-ordinate system was adopted rather than the former rectilinear one. The vortex sheet cast off during flow separation from the upstream lip at the entrance to the expansion will be cylindrical and subsequently will roll up into a train of vortex rings or toroids, having a circular generator with radius R. This then represents the origin of the toroidal co-ordinates adopted for describing the fluid motion associated with the ring vortices. Provided the vorticity is concentrated in the area relatively close to the generator compared with its radius R, its distribution, together with that of the potential velocity field surrounding it, will be similar in many respects to that of the modified Rankine vortex adopted in references [14, 17]. The expansion chamber flow is fully confined in both chamber and pipe while the principle acoustic motion is also in the same axial direction as the flow, rather than being directed across it [13, 14]. Finally, the vortices travel along a path in the expansion chamber that is now at least an order of magnitude longer in relation to their core diameter, than before. However, recalling that once generated vorticity is known to persist for relative long distances as it is convected with the flow, the relative increase in length of this path may remain a less significant factor, so long as any consequences of the diffusion of vorticity are taken into account [17] during the modelling.

The physical description should logically begin with setting out the essential features of the steady and fluctuating velocity patterns in the chamber and tailpipe. This is an essential preliminary to establishing their combined acoustic behaviour [16–18]. Following this, in accordance with earlier discussion, the development of the periodic sequence of toroidal vortices is described in appropriate detail [17]. This includes the dynamics of their development from the initial cylindrical vortex sheet created by flow separation at the chamber entrance. Previous detailed measurements combined with the associated analytical framework [13, 14, 17] give useful guidance here. The motion of the ordered train through the chamber is described next, followed by the dynamics of the interaction at the tailpipe entrance, again taking full advantage of existing knowledge [13, 14, 17]. Finally, the sequence is completed by a description of the total velocity field existing within the tailpipe and those factors governing sound power emission [18] from its open end.

2.1. THE TOTAL VELOCITY FIELD IN THE CHAMBER AND TAILPIPE

The essential features of the flow patterns normally observed in a number of geometrically similar expansion chambers are reproduced in Figure 1. Although the representation has been deliberately simplified, conservation of mass, momentum and

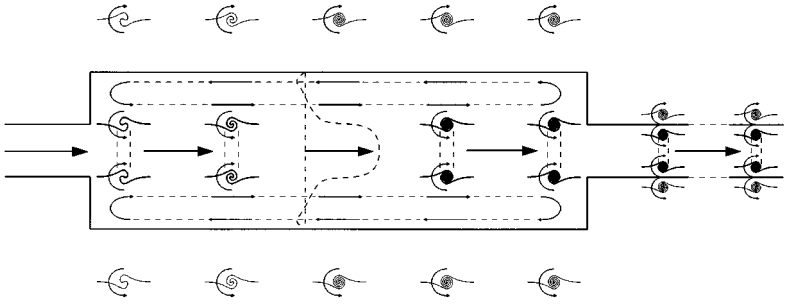

Figure 1. Expansion chamber/tailpipe flow distribution. Showing (1) separating cylindrical free shear layer rolling up into ring vortices; (2) principal image vortices; (3) mean velocity profile; and (4) flow reversals and outer circulation.

circulation were fully satisfied during the development, as was conservation of total energy including any acoustic energy radiated to the surroundings, etc. Furthermore, all the factors that are of physical significance in the present context are retained, while other far less significant ones have been omitted for simplicity. For example, the solenoidal velocity fields at the walls that remain in stable equilibrium with the axial static pressure gradients have been omitted. The existence of a continuous core of plug flow shown extending along the axis of the expansion from inlet to outlet is realistic. As well as conforming with observation, this distribution satisfies conservation of mass across each plane along the expansion including the entrance and exit pipe orifices, the confining influence of the chamber boundaries, with the existence of the recirculating flow that is essential to satisfy the boundary conditions on its end walls. Thus, there is an annular region of reversed flow extending along the outer boundary of the chamber that is separated from the core flow by an annular region of sheared mixing layer flow, where the vorticity shed at the inlet lip of the expansion is concentrated. Further, confirmation of the realism of this representation is provided by the close agreement obtained between the static pressure loss calculated with this flow distribution model and that observed experimentally. In both cases, this was found to increase linearly at almost identical rates with the axial length of the chamber. Also, both measured and calculated loss remain essentially independent of the area contraction ratio. This is clearly not the case when the core flow expands to occupy more than the central region of the expansion.

Included in Figure 1 are the vortex sheets that roll up under the influence of the resonant acoustic fields of the tailpipe into a train of discrete toroidal vortex rings [17] repeated periodically at the resonant frequency f_r. These are represented symbolically by the four vortex rings shown spaced more or less evenly along the chamber axis, each with a circulation Γ_v. Obviously [17], an equivalent array of images, each with circulation Γ_i that just cancels the potential field of the inner set must be present also, to satisfy the conditions for zero flow across the solid boundaries. Such confined flow behaviour differs markedly from that of a free jet, since the combined influence of the cylindrical boundary and the image vortices together generates a potential field that has a tendency to restrain radial expansion of the rings, and similarly any changes in the radial distribution of the time-averaged axial flow velocity in the shear layer surrounding the central core flow as well as constraining this flow. Finally, the expected persistence of the vortices as they convect with the mean flow is also demonstrated in Figure 1 by their continued presence in the tailpipe, which is also in accordance with observation.

2.2. VORTEX DYNAMICS REVISITED

The total velocity field vector $\mathbf{v}$ describing the distribution of velocity in the expansion and tailpipe in Figure 1 can be described [4, 14, 17] as the sum of an irrotational field and a solenoidal field. The former derived from a scalar potential ϕ, that has a time-average value $\bar{\phi}$ and also a fluctuating part ϕ', that is largely associated with the acoustic wave motion. The other field represents the rotational motion mainly associated with the vorticity in the flow that can be derived from a vector potential $\mathbf{A}$. So by definition one has

$$\mathbf{v} = \nabla\phi + \nabla \wedge \mathbf{A}, \tag{4}$$

where the solenoidal part of the velocity field $\nabla \wedge \mathbf{A}$ is induced by the vorticity vector $\mathbf{\Omega} = \nabla \cdot \mathbf{v}$. Direct measurement of vorticity has proved difficult to accomplish, so it must often be inferred using other methods [14, 17]. The overall field $\mathbf{v}$ is also the sum of a time-averaged part $\bar{\mathbf{v}}$ and fluctuating part $\mathbf{v}'$ as does the total vorticity vector $\mathbf{\Omega} = \bar{\mathbf{\Omega}} + \mathbf{\Omega}'$.

Assuming that the Kutta condition is satisfied during flow separation at the upstream lip, the cylindrical vortex sheet representing the shear layer leaves it in a direction parallel to the pipe and chamber axis. It can then be easily shown [14, 17] that, if one neglects the pipe boundary layer, the time-average rate of shedding circulation Γ to form this sheet is expressed by

$$\mathrm{d}\Gamma/\mathrm{d}t = 0{\cdot}5U^2, \tag{5}$$

where U is the time-averaged axial flow velocity in the inlet pipe. When, as indicated in Figure 1, this inherently unstable sheet rolls up into a periodic train of toroidal vortices [17] during flow-excited resonance at a frequency f_r, the circulation carried by each ring, or their individual strengths, has an average value given by

$$\Gamma_v = 0{\cdot}5U^2/f_r. \tag{6}$$

To produce the simplest model of such a ring to analyze, Kelvin [19] assumed that the resulting vorticity ω_t, tangential to the generator, is uniformly distributed over a torus or "anchor ring" that has a radius r_c. Provided that the ratio of torus radius to anchor ring radius, $r_c/R \ll 1$, this does provide an approximation to better than first order in an ideal fluid [20] both to the vorticity distribution in the torus or core, and to the distribution of the associated velocity potential in the surrounding irrotational circulation. In a real fluid, a more appropriate approximation to the distribution of vorticity around the generator [14, 21] is given by

$$\Omega_t = [\Gamma_v/\pi r_c^2]\exp(-r^2/r_c^2). \tag{7}$$

The influence of viscous diffusion [19] will cause the core radius r_c to increase at a rate proportional to $(4vt)^{0{\cdot}5}$, where v is the kinematic viscosity and t the lifetime of the ring. Conservation of angular momentum is satisfied for the ring if total circulation remains invariant. To allow for vortex stretching [17, 21] the torus volume which is proportional to Rr^2 should also remain consistent to first order, so that during its convection down the axis of the expansion, the core radius varies according to

$$r_c^2 \propto 4vtR_0/R, \tag{8}$$

where R_0 is the initial radius of the ring. The axisymmetric velocity field in the vicinity of an isolated vortex ring can be found from the stream function ψ which satisfies the continuity equation. Lamb [19] has shown that the velocity at a point P remote from the core of

Kelvin-type vortex can be found from the stream function expressed in cylindrical co-ordinates as

$$\psi = (\Gamma/4\pi)(r_1 + r_2)[\mathrm{K}(\alpha) - \mathrm{E}(\alpha)], \tag{9}$$

where r_1 and r_2 are, respectively, the shortest and longest distances from the point P to the ring generator, $\alpha = (r_2 - r_1)/(r_2 + r_1)$, and $\mathrm{K}(\alpha)$ and $\mathrm{E}(\alpha)$ are, respectively, the complete elliptic integrals of the first and second kinds. For a given Γ_v and radial dimensions of the expansion, one can allocate an appropriate strength and position to Γ_i, noting that Γ_i must have the circulation in the opposite sense to Γ_v.

2.3. THE MEAN ACOUSTIC ENERGY FLUX

With a homentropic flow, where the total velocity field is described by equation (4), Doak [1] has demonstrated that the dominant mechanism for the production of mean energy flux associated with the enthalpy fluctuations, of which the acoustic energy constitutes a part, is by the action of a Coriolis force, derived from the corresponding Coriolis acceleration $(\mathbf{v} \times \mathbf{\Omega})'$, working on the fluctuating flow. The result can be expressed for each frequency of interest by

$$\nabla_1 \overline{H'(\rho\mathbf{v})f'} = -\overline{(\rho\mathbf{v})'(\mathbf{\Omega} \times \mathbf{v})f'}, \qquad H = h + \tfrac{1}{2}\mathbf{v}^2, \tag{10}$$

where H is the stagnation enthalpy per unit mass, $h = E + p/\rho$, and E is the internal energy, p the pressure and ρ the mass density. When this is applied to the flow distribution in Figure 1, it seems clear that ω_t will be the dominant component of vorticity. Also excepting the area discontinuities at the inlet and outlet ends of the expansion, where sets of evanescent waves are present [16], the corresponding irrotational velocity fluctuations are predominately axial, with a maximum amplitude at each of the resonant frequencies of the chamber/tailpipe combination.

Once a value of the core radius r_c has been established, Ω_t can be evaluated with equation (7), combined with equation (6). The core radius may be estimated from shear layer velocity profile measurements, or inferred [14] from velocity fluctuations observed in the shear layer. Alternatively, it can be estimated from other data [17, 22]. Having then established or estimated the characteristic features of the toroidal vortex rings, for example, their radius must be close to that of the inlet pipe, the relevant components of the solenoidal velocity field at the upstream and downstream edges of the expansion can be calculated [19] with equation (9). The abundance of relevant data now available in the literature, combined with the results of previous studies [4, 10, 17], allows a fair estimate to be derived describing the corresponding irrotational field. These can then be combined and substituted into equation (10) to calculate a fair estimate of the sound power generation at the discontinuities. The results of this will be compared later with precise measurements [18] of the acoustic power flux in the downpipe, the chamber, the tailpipe and finally the radiated field. Detailed measurements of the velocity field using non-invasive optical techniques [14] would have provided a further check on the realism of the estimates of the characteristics of the velocity fields in the chamber, but the appropriate facilities were not available. On the other hand, the aim was to develop predictive software that did not require such detailed velocity field measurements, but relied on existing information, for example, references [4, 8–13, 16, 17].

Reliable estimates of the coherent sound power flux were obtained [18] from measurements with pairs of flush-mounted carefully calibrated wall microphones. The pressure signals were recorded on to a multi-track digital tape recorder, which was then

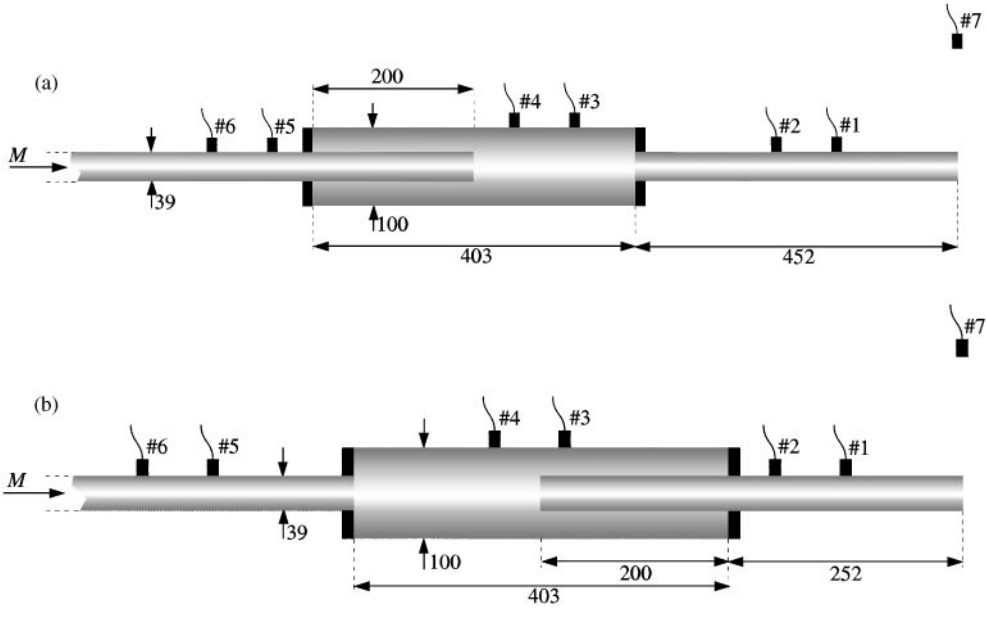

Figure 2. Expansion chambers with microphone positions; (a) No. 1 with inlet sidebranch; (b) No. 2 with outlet sidebranch.

played back into a multi-channel computer data acquisition system and stored as 16-bit data. Subsequent processing and analysis was carried out using custom-written code on a 200 MHz RISC computer. This was used first to evaluate the complex spectral amplitudes of the forward and backward acoustic wave components, $\hat{p}^+$ and $\hat{p}^-$, respectively, by appropriate processing [18] of the auto- and cross-spectra derived from each pair of microphones. The net acoustic intensity I, or the acoustic power flux per unit area was then calculated with the well-established expression

$$I = [|\hat{p}^+|^2(1 + M)^2 - |\hat{p}^-|^2(1 - M)^2]\rho_0 C_0 \tag{11}$$

One notes that in a highly reactive acoustic field [18] the amplitudes of the pressure components $\hat{p}^+$ and $\hat{p}^-$ are almost equal and so the net power flux is often a small proportion of the total fluctuating acoustic energy.

The coherent intensity was calculated by multiplying the intensity spectrum defined in equation (11) by the coherence of the cross-spectrum between the relevant pair of microphones signals. The coherent-radiated sound power was calculated similarly from the measured total power, by its product with the coherence of the tailpipe/free-field cross-power spectrum. Coherent power flux was chosen in preference to the total power, as it was considered that this was more closely associated with the acoustic energy flux arising from sustained excitation by the flow.

Previous parametric studies [10, 12, 16] of the influence of mean flow Mach number and of some geometrical features on noise generation by a series of typical intake/exhaust system elements, including expansion chambers, had been restricted to spectral measurements of the total radiated power. Subsequently, appropriate source/system models [4, 10, 12] were developed to fit these results. Usually, as might be expected, a source position at the tailpipe/expansion chamber junction was found to give the most consistent

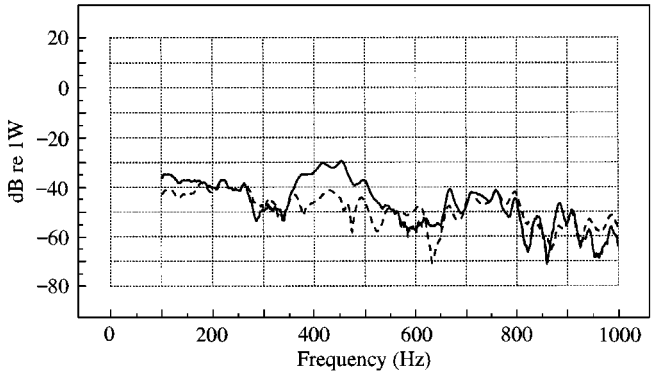

Figure 3. Coherent power flux measured in downpipe - - - -, with chamber 1; —— with chamber 2.

match. The new measurements reported here provide an opportunity to investigate this assumption and also to clarify further the roles of both inlet expansion and outlet contraction in the basic sound-generating mechanisms. Furthermore, local power flux measurements allow one to investigate the influence of local changes in geometric detail, such as the addition of an annular sidebranch to either the inlet, or outlet pipe/chamber junction [16]. These two alternative geometries are illustrated in Figure 2 with the positions of the microphone pairs. In both examples tailpipe and chamber resonances occur at integer multiples of 365 and 440 Hz, respectively, while those for both sidebranches occur at odd integer multiples of 425 Hz. Thus, the first resonant frequency of the two chambers lies close to that of the annular sidebranches.

3.1. SOUND POWER FLUX MEASUREMENTS

The coherent sound power flux spectra, measured at a mean flow Mach number equal to 0·2 in the downpipe leading to each chamber, are compared in Figure 3. The comparisons show that these power spectra have closely similar spectral levels except over a band about 150 Hz wide centred at 425 Hz, where the levels in the downpipe of chamber 2 exceed those of chamber 1, by around 10 dB. This difference can be explained by the presence of the sidebranch at the inlet end of chamber 1, as presumably, its first resonance opposes or "cancels" that of the chamber. Other examples of a similar change in acoustic behaviour, clearly δ, related to the presence or absence of a sidebranch at the inlet end, were found during the measurements. The oscillations in spectral level above 600 Hz, repeating with an average frequency of 40 Hz, apparently correspond to the overall length of the system representing the combined lengths of downpipe, chamber and tailpipe, in accordance with equation (1).

The coherent power flux spectrum measured in chamber 1 is plotted with the corresponding measured tailpipe power spectrum in Figure 4(a) and those similarly for chamber 2 in Figure 4(b). Comparing the chamber power flux levels for chamber 1 with the corresponding downpipe levels in Figure 3 shows that they also correspond closely except for two rather narrow bands centred at 375 and 475 Hz where the peak level increased by around 7 and 20 dB respectively. Both downpipe and chamber levels were almost identical at 425 Hz, the inlet sidebranch first resonance. A repetition of this comparison for chamber 2 again reveals a somewhat similar correspondence of power flux levels, firstly below

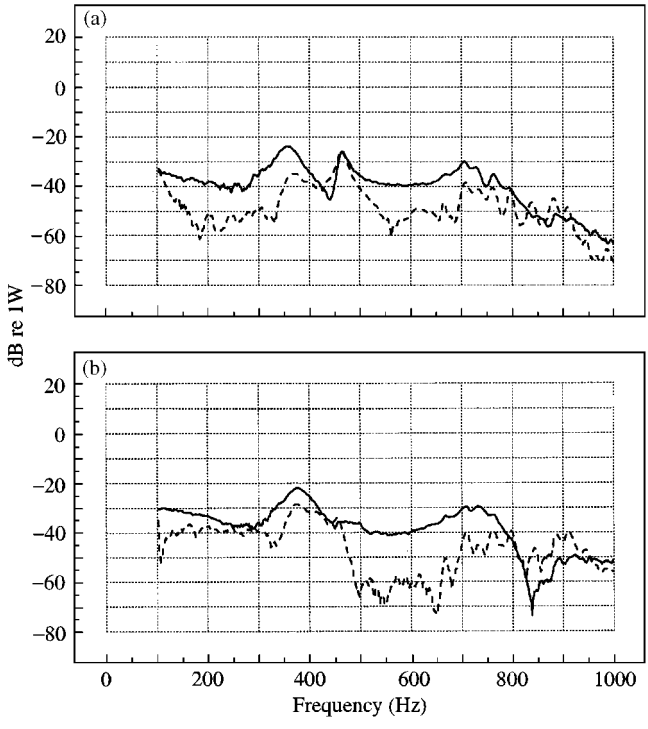

Figure 4. Measured coherent power flux; (a) for chamber 1; (b) for chamber 2; —— in tailpipe, - - - - in chamber.

275 Hz, then between 375 and 475 Hz and finally above 550 Hz. Otherwise, there was an increase in level of some 8–10 dB between 275 and 375 Hz, with a sharp decrease in level of 20 dB below that in the tailpipe at 475 Hz. These differences between the two chamber power flux level spectra clearly relate to the changes in reverberant acoustic behaviour at the chamber inlet and outlet, while these can also be directly associated with the repositioning of the annular sidebranches.

Returning to Figure 4(a), a comparison between the power flux spectral levels measured in chamber 1 and its tailpipe reveals a general increase of from 10 to 15 dB in tailpipe power flux below 370 Hz and also between 525 and 750 Hz, reducing to zero above this frequency and over the band between 370 and 525 Hz. This last feature maintains the pronounced dip in power level measured in the chamber at 425 Hz, the inlet sidebranch first resonance. The comparison for chamber 2 in Figure 4(b) reveals a similar behaviour below 370 Hz, though the level increase is some 5–10 dB less. This increase then falls from 7 dB at 370 Hz to zero by 450 Hz, increasing sharply again at 475 Hz to 20 dB and maintaining that level of increase to around 750 Hz, finally reducing rapidly to zero above this frequency. Comparing the two tailpipe coherent sound power flux levels in Figure 4(a) and (b) reveals that below 300 Hz, the level with chamber 1 lies from 0 to 5 dB above that with chamber 2. Then from 300 to 370 Hz, the two levels are very close. From 370 to 450 Hz the measured levels in chamber 2 tailpipe are some 5 dB higher than those in chamber 1. However, above 440 Hz the tailpipe level of chamber 1 rises some 15 dB to a peak at 475 Hz, while that for chamber 2 remains at a constant level some 10 dB below this peak. Thus the situation has reversed again, so the level in the tailpipe of chamber 1 exceeds that in the other tailpipe by an amount varying between 5 and 10 dB from 460 Hz or so to 540 Hz. Above this the two levels remain close up to 800 Hz.

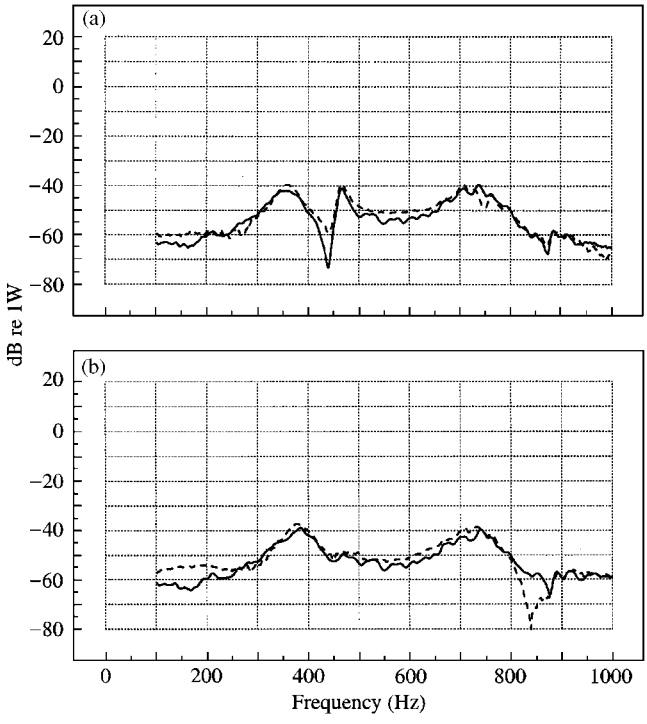

Figure 5. Radiated coherent power; (a) with chamber 1; (b) with chamber 2; —— measured in free field, - - - - predicted from tailpipe power flux.

The coherent acoustic power spectra radiated from the open pipe-end and measured with chambers 1 and 2 are plotted as Figure 5(a) and (b) respectively. They are both accompanied by a radiated power prediction calculated [18] from the corresponding measured coherent power flux in the tailpipe. The two measured radiated sound power spectra remain in close agreement up to 900 Hz, with the exception of the band between 350 and 500 Hz, where the differences in level correspond to those just described for the two tailpipes. The results in both Figure 5(a) and (b) show that above 200 Hz or so, the predicted power spectra are in fair agreement with the measured ones, the discrepancies being larger at the lower power levels. Recalling that the measured power flux in the tailpipe and chamber is but a small proportion of the total fluctuating power in these highly reactive elements, the close agreement between measured and predicted power at the higher levels provides a useful indication of the precision of the measurements of power flux made within the pipes and chamber. This was achieved in spite of the contamination of the acoustic pressure signals by boundary layer and other unrelated pressure fluctuations at the wall.

In summary, the measurements with chamber 1 and with chamber 2 revealed that there were significant sources of flow noise generation at the chamber outlet/tailpipe junction centred at the first two tailpipe resonances, with sound power levels at least one to two orders of magnitude above the general background flow generated noise. There was a further similar source with chamber 1 at the junction of the chamber/inlet sidebranch at 475 Hz, that was presumably associated with the resultant interaction between chamber, sidebranch and tailpipe resonances. Power flux measurements above 1000 Hz revealed the existence of a third source at 1100 Hz with chamber 2 but not with chamber 1. This source, corresponding to the third tailpipe resonant frequency, had a sound power that was some two orders of magnitude below the first two.

3.2. THE CALCULATIONS

The total measured sound power radiated by chamber 1 calculated from the spectral measurements in Figure 5 is just under 25 mW, while that for chamber 2 was just over 30 mW, when the mean flow Mach number was 0·2. At 365 Hz and $M = 0{\cdot}2$, from equation (6) the circulation carried by each vortex has a value approximately equal to 6·7 m^2/s, while at 730 Hz this is halved to 3·3 m^2/s. Observations on free shear or mixing layers, for example references [22, 23], suggest that the r.m.s. level of axial and radial velocity fluctuations are around 10 percent of the mean jet velocity. Assuming a parallel situation exists in the expansion chamber then one could assume equivalent fluctuating velocities. Furthermore, these have a spectrum in the middle of the mixing layer that is flat up to a Strouhal number of 0·5, or around 1800 Hz in the present case. At $M = 0{\cdot}2$ this suggests that the velocity fluctuations have a spectral amplitude equal to 4 mm/s r.m.s., on average, at least at 365 and 730 Hz, where the Strouhal numbers are of order 0·1 and 0·2 respectively. Assuming a core radius of 6 mm and substituting this value into equation (7) suggests that ω_t is of order 60 000. Finally, inserting these values into equation (10) to calculate the corresponding average sound intensity, suggests the narrowband sound power generated at the tailpipe/chamber junction is around 13 mW, equivalent to a spectral level of -19 dB relative to 1 W. This seems to be of similar order to the measured peak sound power level of -22 dB or thereabouts.

4. DISCUSSION

These measurements provide new information to add to the results of earlier parametric studies of flow noise generation by expansion chambers. Other measurements [10] suggest that below the frequency of cut-on for higher order modes, or plane wave motion, the total sound intensity is proportional to $M^{4{\cdot}5}$ to a fair approximation and is also proportional to $(x/a)^{-4{\cdot}25}$, $4 < x/d < 12$, where d is the internal diameter of the inlet and outlet pipes and x the length of their separation. These new measurements confirm the assumption [10, 12] that fluctuating Coriolis forces are concerned with one major source of flow generated noise, at the chamber outlet/tailpipe junction. Presumably, a similar mechanism is also concerned in noise produced at a chamber inlet/sidebranch junction.

ACKNOWLEDGMENTS

The work represents part of the studies on sources of flow-induced pressure pulsations in pipe systems transporting compressible fluids supported by the Engineering and Physical Sciences Research Council Grant K/79994.

REFERENCES

1. P. E. DOAK 1998 *Theoretical and Computational Fluid Dynamics* **10**, 115–133. Fluctuating total enthalpy as the basic generalised acoustic field.
2. P. O. A. L. DAVIES and P. E. DOAK 1990 *Journal of Sound and Vibration* **138**, 345–350. Wave transfer to and from conical diffusers.
3. P. E. DOAK 1992 *Journal of Sound and Vibration* **155**, 545–548. Acoustic wave propagation in a homotropic, irrotational, low Mach number mean flow.
4. P. O. A. L. DAVIES 1996 *Journal of Sound and Vibration* **190**, 345–362. Aeroacoustics and time varying systems.

5. LORD RAYLEIGH 1896 *The Theory of Sound* (two volumes). London: Macmillan: second edition, vol. II, Chapter XXIII. Vortex motion and sensitive jets.
6. G. B. BROWN 1937 *Proceedings of the Physical Society* **49**, 493–507, 508–521. Vortex motion causing edge tones. The mechanism of edge tones.
7. A. WOOD 1940 *Acoustics*. London: Blackie, see Chapter XV: Organ Pipes.
8. D. ROCKWELL 1983 *American Institute of Aeronautics and Astronautics Journal* **21**, 645–664. Oscillations of impinging shear layers.
9. E. NAUDASCHER and D. ROCKWELL 1994 *Flow Induced Vibrations*. Rotterdam: Balkerna.
10. P. O. A. L. DAVIES 1981 *Journal of Sound and Vibration* **77**, 91–209. Flow–acoustic coupling in ducts.
11. M. NAKANO 1991 *Internoise* **91**, 545–548. Self-sustained flow oscillations in a silencer with a single expansion chamber.
12. P. O. A. L. DAVIES and K. R. HOLLAND 1999 *Journal of Sound and Vibration* **223**, 425–444. IC engine intake and exhaust noise assessment.
13. P. A. NELSON, N. A. HALLIWELL and P. E. DOAK 1981 *Journal of Sound and Vibration* **78**, 15–38. Fluid dynamics of flow induced resonance, Part I: experiment.
14. P. A. NELSON, N. A. HALLIWELL and P. E. DOAK 1981 *Journal of Sound and Vibration* **91**, 375–402. Fluid dynamics of flow induced resonance, Part II: flow–acoustic interaction.
15. T. D. MAST and A. D. PIERCE 1993 *Journal of the Acoustical Society of America* **97**, 163–172. Describing function theory for flow excitation of resonators.
16. P. O. A. L. DAVIES 1996 *Journal of Sound and Vibration* **190**, 677–712. Piston engine intake and exhaust system design.
17. P. O. A. L DAVIES, J. HARDIN, A. V. J. EDWARDS and J. P, MASON 1975 *American Institute of Aeronautics and Astronautics Paper No*. 75–441. A potential flow model for the calculation of jet noise.
18. K. R. HOLLAND and P. O. A. L. DAVIES 2000 *Journal of Sound and Vibration* **230**, 915–932. The measurement of sound power flux in flow ducts.
19. H. LAMB 1932 *Hydrodynamics*, 59–94. New York: Dover; sixth edition, reissue 1961.
20. L. E. FRAENKEL 1972 *Journal of Fluid Mechanics* **51**, 119–135. Examples of steady vortex rings of small cross section in an ideal fluid.
21. T. E. BASE 1969 *Ph.D. Thesis, University of Southampton*. Mathematical studies of vortex models to represent unsteady fluid flow.
22. J. C. LAU, P. J. MORRIS and M. J. FISHER 1979 *Journal of Fluid Mechanics* **93**, 1–27. Measurements in subsonic and supersonic free jets using a laser velocimeter.
23. N. W. M. KO and P. O. A. L. DAVIES 1971 *Journal of Fluid Mechanics* **50**, 49–78. The near field within the potential core of subsonic cold jets.